International Journal of Undergraduate Research and Creative Activities

Volume 7 | Issue 1 Article 4

October 2023

The Photophysical Properties of CdTe/ZnS Core/Shell Quantum Dots

Christopher Z. Eddy
eddy6081@pacificu.edu

Hayley M. Johanesen
joha0746@pacificu.edu

James J. Butler
jjbutler@pacificu.edu

David B. Cordes
cordes@pacificu.edu

Recommended Citation

Eddy, Christopher Z.; Johanesen, Hayley M.; Butler, James J.; and Cordes, David B. (2023) "The Photophysical Properties of CdTe/ZnS Core/Shell Quantum Dots," *International Journal of Undergraduate Research and Creative Activities*: Vol. 7: Iss. 1, Article 4.
DOI: 10.7710/2168-0620.1057
Available at: https://digitalcommons.cwu.edu/ijurca/vol7/iss1/4

The Photophysical Properties of CdTe/ZnS Core/Shell Quantum Dots

Peer Review
This work has undergone a double-blind review by a minimum of two faculty members from institutions of higher learning from around the world. The faculty reviewers have expertise in disciplines closely related to those represented by this work. If possible, the work was also reviewed by undergraduates in collaboration with the faculty reviewers.

Abstract
The distinctive fluorescent properties of semiconductor nanocrystal quantum dots (QDs) make them advantageous for use in optoelectronic and biological applications. We report on experiments done to characterize the optical properties and the general photostability of CdTe QDs with varying ZnS shell thicknesses. Steady-state and time-resolved absorption and fluorescence spectroscopy measurements indicate that increasing the ZnS shell thickness results in longer absorption and emission wavelengths, increased quantum yield, and improved photostability.

Keywords
Quantum Dots, Fluorescence, Photobleaching

Acknowledgements
We want to thank the M.J. Murdock Charitable Trust, the Pacific University Holce Endowment, and the Pacific Research Institute for Science and Mathematics for funding this work. Additionally, TEM was performed at Portland State University's Center for Electron Microscopy and Nanofabrication.

Editor's Note: Dr. James J. Butler, Ph.D., Professor, Department of Physics, Pacific University, and Dr. David B. Cordes, Associate Professor, Department of Chemistry, Pacific University, served as the faculty mentors for this work.

INTRODUCTION

Nanoparticle research has been flourishing since these materials were first synthesized in the 1980s (Eustis & El-Sayed, 2006). Investigations of these nanometer-sized fluorescent particles have involved the interdisciplinary collaboration of chemists, physicists, materials scientists, and biologists. Nanoparticle materials have been employed in a variety of electronic and optical devices, while recent research has led to a range of new applications in medicine, diagnostics, and genomics. (Kramer & Sargent, 2014; Yao, Yang, & Duan, 2014). Quantum dots (QDs), sometimes referred to as colloidal quantum dots, are a subclass of semiconductor nanoparticles with particularly interesting properties. Their diameter ranges from 1-10 nm, and they usually have a narrow size distribution, a high quantum yield, and an easily-tunable, narrow emission wavelength range (Zhang, Chen, Wang, Ye, & Zhong, 2009). For these reasons QDs are more attractive to use than traditional organic fluorophores that tend to have broad emission wavelength ranges.

It has been shown that the photostability and photoluminescence of QDs can be improved by growing an inorganic semiconductor shell of a wider bandgap around the semiconductor core, yielding core/shell QDs (Hines & Guyot-Sionnest, 1996; Dabbousi et al., 1997). In this paper, we report on a study of cadmium telluride/zinc sulfide core/shell quantum dots (CdTe/ZnS QDs). This investigation focuses on the effect of shell thickness on a full range of optical properties including absorption, emission, fluorescence lifetime, quantum yield, and photostability. This fills an important need in core/shell QD research as there have been few reports of this kind of broad optical study (Xu et al., 2011).

RESULTS AND DISCUSSION

The CdTe/ZnS QDs were synthesized using standard techniques as discussed in the experimental section of this paper. Core/shell QDs were analyzed up to approximately two ZnS monolayers, as literature suggests that thicker ZnS shells lead to the formation of defects that decrease the quantum yield and the stability (Smith, Mohs, & Nie, 2009; Talapin, Mekis, Gotzinger, Kornowski, Benson, & Weller, 2004). Samples with approximately three ZnS monolayers were also synthesized but results were inconsistent and not significantly different than those for two monolayers. The QDs were then characterized in terms of size and optical properties. Optical measurements included absorbance and fluorescence spectroscopy, quantum yield, fluorescence lifetime, and photostability. Additional characterization was conducted using transmission electron microscopy.

Absorbance

Each QD sample was diluted to an absorbance of 0.1 at the excitonic peak to eliminate concentration differences between the samples and avoid inner filter effects. Figure 1 shows typical normalized absorbance spectra for QDs with various numbers of shell coatings. The wavelengths

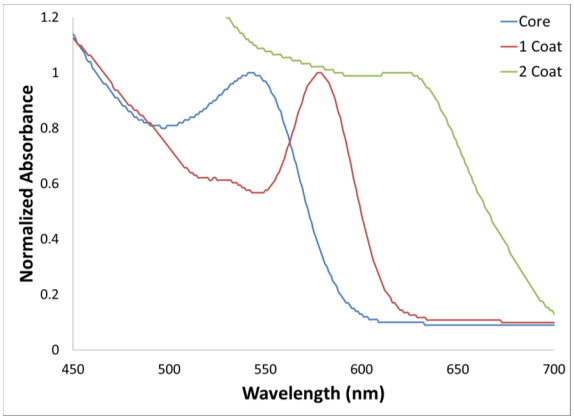

Figure 1. Absorbance spectra for CdTe/ZnS QDs with various numbers of shell coatings.

https://digitalcommons.cwu.edu/ijurca/vol7/iss1/4
DOI: 10.7710/2168-0620.1057

DOI: http://dx.doi.org/10.7710/2168-0620.1057

of the absorption peaks ranged from 543 to 618 nm with a larger ZnS shell thickness generally resulting in a longer wavelength.

As a classic type-I system, CdTe/ZnS QDs are expected to show little sensitivity to increasing shell thickness because the bandgap of the CdTe core lies within the much larger bandgap of the ZnS shell. However, the red-shifting of the CdTe/ZnS QD absorbance peaks with increasing shell thickness in our experiments was quite significant and cannot be fully explained by simple leaching of the exciton into the surrounding ZnS matrix, a phenomenon associated with red-shifts of ~10 nm or less (Dabbousi et al., 1997). Instead, the large shift observed on addition of each of the ZnS shells is most likely caused by some formation of a CdS layer at the interface between the CdTe core and ZnS shell. Indeed, recent work on CdTe/CdS QDs suggests that Ostwald ripening processes acting on the core Cd-Te bonds make Cd^{2+} ions available for reaction with S^{2-} at the core/shell interface (Jing et al., 2015). The formation of a type-II interaction between the CdTe core and a CdS layer is one possible explanation for the observed red-shifting. It is also possible that some degree of alloying is occurring at the core/shell interface producing ZnCdTe species that contribute to red-shifted spectra (Ivanov et al., 2007).

Fluorescence Emission

Fluorescence spectra of the QD samples were observed and recorded. Under UV illumination the color of the fluorescence emission was observed to be green for the core-only sample, orange for the 1 coat ZnS sample, and red for the 2 coat ZnS sample. Figure 2 shows typical normalized fluorescence emission spectra for QDs with various numbers of shell coatings. The wavelengths of the fluorescence emission peaks ranged from 564 to 642 nm with a

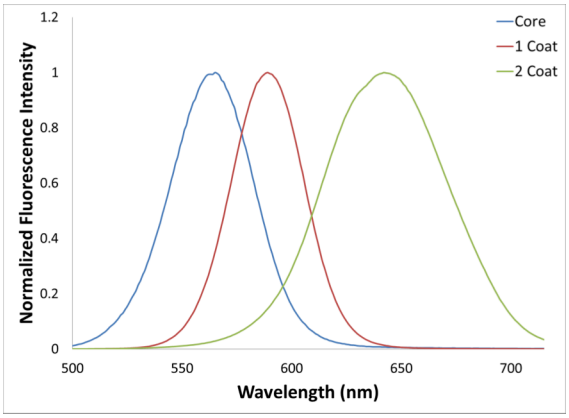

Figure 2. Fluorescence emission spectra for CdTe/ZnS QDs with various numbers of shell coatings.

larger ZnS shell thickness generally resulting in a longer wavelength. The red-shift in wavelength was most dramatic between the 1 coat ZnS and 2 coat ZnS samples. This red-shift is consistent with leaching of the exciton into the ZnS shell (Dabbousi et al., 1997) but could also be attributable to CdS layer formation or alloying as discussed in the absorbance section.

Quantum Yield

The absolute quantum yields (QYs) were determined using Rhodamine 6G in ethanol as the standard. This produced typical values of 0.7%, 1.4%, and 3.6% for the core-only, 1 coat ZnS, and 2 coat ZnS samples, respectively. Although these values are fairly low, they do indicate a trend of increasing QY with increasing thickness of the ZnS shell. This trend is seen in Figure 3, which shows typical values of the relative QY for QDs with various numbers of shell coatings.

It should be noted that these results are for a single set of QDs, so we do not have enough data to accurately assess the uncertainties due to sample-to-sample variations. However, if the trend shown in Fig. 3 is valid, one possible explanation of the increase in QY with increasing shell

DOI: http://dx.doi.org/10.7710/2168-0620.1057

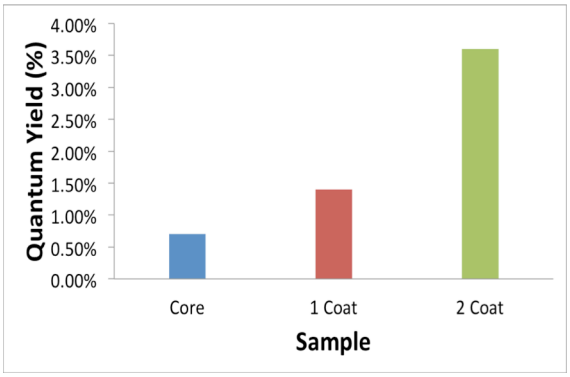

Figure 3. Quantum yield for CdTe/ZnS QDs with various numbers of shell coatings.

thickness is the passivation of surface defect sites (Hines & Guyot-Sionnest, 1996) and the increased protection of the core from oxygen, which can quench fluorescence (Zhang et al., 2009). These results also show that the maximum QY occurs with the 2 coat ZnS sample. This is consistent with previous research that found that the peak fluorescence efficiency occurs at about 2.5-3 monolayers (Smith et al., 2009).

Transmission Electron Microscopy (TEM)

TEM was used to determine the QD diameters and lattice fringe spacing (*d*-spacing). Figure 4 shows TEM images of QDs with various numbers of shell coatings. The presence of lattice fringes show that the QDs were crystalline. Crisscrossed lattice fringes in the CdTe core sample are indicative of the overlapping of multiple CdTe QDs (Waitz, Rentenberger, & Karnthaler, 2009).

Figure 5 shows the sample-to-sample variation in the size distribution of the QDs. The width of the distributions for the coated QDs may be attributable to inconsistent stirring during the synthesis leading to certain QDs being coated with thicker ZnS layers than others. Table 1 shows the measured diameter and standard deviation based on the QD data from Fig. 5. As expected, the QDs with the largest number of ZnS coatings were measured to have the largest diameters.

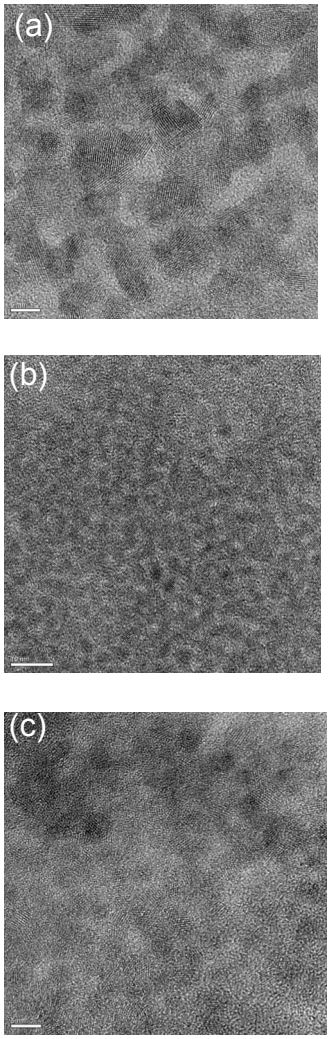

Figure 4. TEM images of CdTe/ZnS QDs with (a) core only, (b) 1 coat ZnS, (c) 2 coat ZnS. Size scale bars in images are as follows: (a) 5 nm, (b) 10 nm, (c) 5 nm.

The measured core-only sample size data was compared with an empirical relationship that has been developed for predicting CdTe QD core diameters based on their absorbance properties (Yu, Qu, Wenzhuo, & Peng, 2003):

$$D = (9.8127\times10^{-7})\lambda^3 - (1.7147\times10^{-3})\lambda^2 + (1.0064)\lambda - 194.84 \quad (1)$$

where λ is the measured excitonic peak wavelength and D is the theoretical diameter

DOI: http://dx.doi.org/10.7710/2168-0620.1057

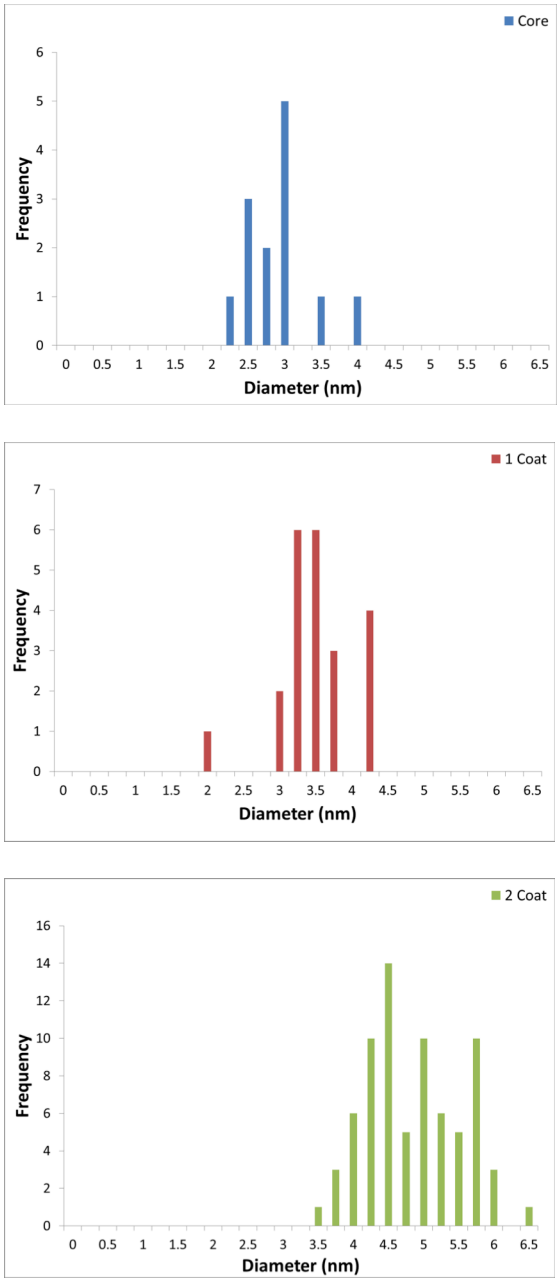

Figure 5. Size distribution of CdTe/ZnS QDs with various numbers of ZnS shell coatings. Y-axis ranges differ to better illustrate the range of QD sizes.

of the QDs, both in nm. The results of this calculation are shown in Table 1. Within experimental uncertainty, the predicted and experimental values are equal to each other for the core-only sample.

The *d*-spacing was measured to be 0.36±0.04 nm, independent of the number of ZnS coatings. An estimate of the number of monolayers of ZnS that make up the coatings on the QDs was done by comparing the experimentally measured diameters of the coated and core-only QDs. The results are shown in Table 1. A ZnS monolayer is *defined* as having a thickness of 3.1 Å because this is the distance between consecutive planes in the bulk wurtzite ZnS lattice (Dabbousi et al., 1997). The data indicate that the thickness of the ZnS layer for each number of coatings on the QDs is consistent with the defined thickness of a monolayer to within experimental uncertainty.

Photostability Studies

Photobleaching is a phenomenon characterized by changes to the optical properties of a fluorophore upon prolonged exposure to light. As our experiments were not performed in a vacuum environment, photobleaching is indicative of photooxidation as well as photodegredation attributed to a high laser power, which are expected to take place together (Nazzal et al., 2004). We measured absorption and fluorescence spectra as well as fluorescence lifetime as a function of incident laser exposure energy in order to determine the photostability of the QDs. Three samples from two different batches were analyzed for the core-only and 1 coat ZnS QDs, while two samples from the same batch were analyzed for the 2 coat ZnS QDs. Note that there was significant sample-to-sample variation in the peak wavelength, absorbance, and emission intensity for the QDs. The observed ranges of these values for the unexposed QDs are shown in Table 2. Because of this variation, data on the exposed QDs were normalized to their initial values so that direct comparisons could be made on any changes to optical properties. In addition, all of the error bars in the figures shown in this section are based on

DOI: http://dx.doi.org/10.7710/2168-0620.1057

Table 1. Experimental and theoretical size data for CdTe/ZnS QDs with various numbers of ZnS shell coatings.

Sample	Measured Diameter (nm)	Standard Deviation (nm)	Calculated Diameter (nm)	Calculated Number of ZnS Monolayers
Core	2.84	0.48	3.2	0
1 coat	3.35	0.51	N/A	1 ± 1
2 coat	4.74	0.69	N/A	3 ± 1

Table 2. Experimentally measured ranges of absorption and emission properties for unexposed CdTe/ZnS QDs with various numbers of ZnS shell coatings.

Sample	Wavelength of Excitonic Peak (nm)	Peak Absorbance	Wavelength of Emission Peak (nm)	Peak Emission Intensity (a.u.)
Core	520-525	0.53-1.87	553-641	6.0×10^{4}-9.5×10^{6}
1 coat	561-608	1.36-2.57	597-634	8.7×10^{6}-1.1×10^{7}
2 coat	617	0.90	655	1.2×10^{7}

sample-to-sample variation, as that was the largest source of experimental uncertainty. However, due to the limited number of samples available, we do not have a high degree of confidence that these error bars are indicative of the true sample-to-sample variation.

Figure 6 shows the measured, normalized wavelength and absorbance of the excitonic peak as a function of incident exposure energy for QDs with various numbers of coatings. Figure 7 shows the measured, normalized wavelength and intensity of the fluorescence emission peak as a function of incident exposure energy for QDs with various numbers of coatings. Note that there is an apparent decrease in normalized wavelength with exposure in some cases. However, given our uncertainty in the error bars based on the limited number of samples and the small differences involved (< 1% change), it is unlikely that these changes are actually significant. In that case, the data indicate that all of the QDs were photostable with respect to wavelength and absorbance over the exposure range considered in this study. However, photobleaching was observed in the fluorescence emission of the QDs as there was a significant decrease in intensity with increasing exposure energy. Interestingly, the degree of photobleaching was reduced with an increasing number of ZnS coatings. Evidently, the thicker coatings serve to protect the QDs, allowing them to maintain higher fluorescence emission intensity after exposure. This is consistent with previous studies that confirmed a decreased photooxidation rate in similar type CdSe/ZnS QDs when the thickness of the capping layer was increased (van Sark et al., 2001). However, the mechanism of photooxidation and dark oxidation in core/shell QDs is still an unresolved issue that needs to be addressed (Nazzal et al., 2004).

Figure 8 shows an example of a measured temporal fluorescence profile for core-only QDs, after baseline subtraction, along with the associated theoretical curve. Theoretical curves were obtained by modeling the fluorescence profiles as a

DOI: http://dx.doi.org/10.7710/2168-0620.1057

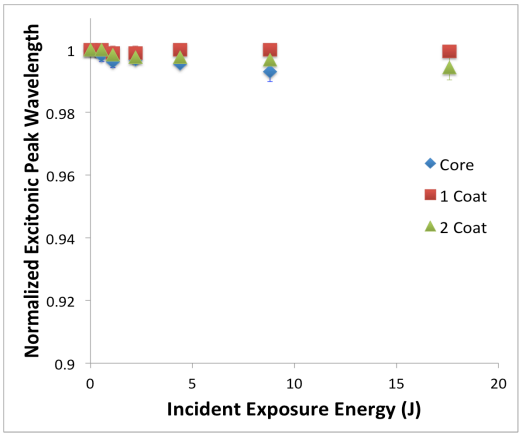

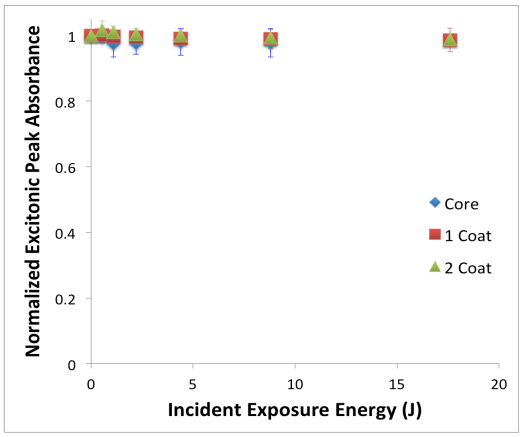

Figure 6. Normalized wavelength and absorbance of the excitonic absorption peak as a function of incident exposure energy for CdTe/ZnS QDs with various numbers of coatings. Unless otherwise indicated, the size of the error bars are given by the size of the marker.

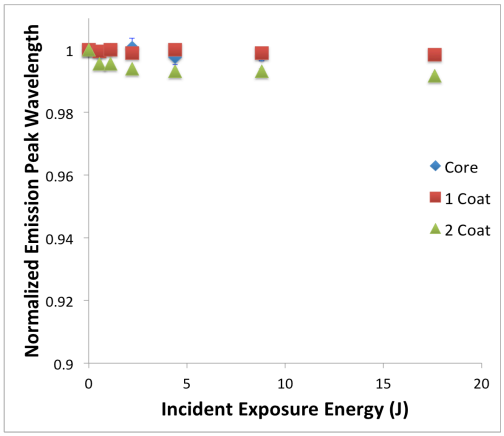

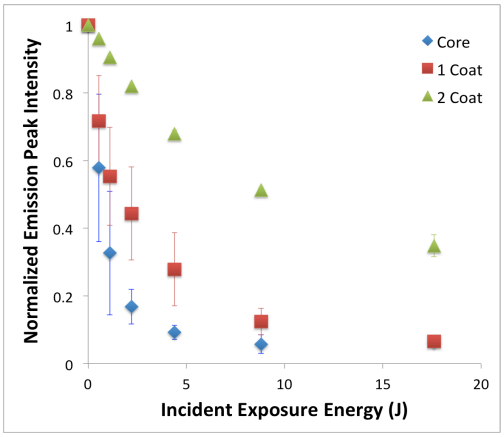

Figure 7. Normalized wavelength and intensity of the fluorescence emission peak as a function of incident exposure energy for CdTe/ZnS QDs with various numbers of coatings. Unless otherwise indicated, the size of the error bars are given by the size of the marker.

convolution of the incident laser pulse profile with a fluorescence decay given by (Demas, 1983):

$$f(t) = \sum_i \alpha_i e^{-t/\tau_i} \qquad (2)$$

where τ_i are the lifetimes and α_i are the corresponding amplitudes of each exponential decay present in the profile. In most cases, it was found that the root-mean-square (RMS) deviation between the measured fluorescence profiles and the model was minimized by assuming a bi-exponential decay, yielding a short component (~1 ns) and a longer component (~20 ns). It is possible that the faster recombination rates may originate from

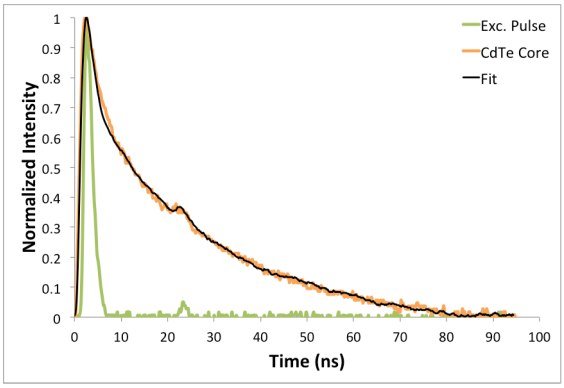

Figure 8. Fluorescence temporal profile of core CdTe QDs (orange), theoretical fit to the data (black), and excitation pulse (green).

delocalized trap-states in surface defect sites at the core/shell interface (Hines & Guyot-

DOI: http://dx.doi.org/10.7710/2168-0620.1057

Sionnest, 1996). In order to determine the accuracy of the best-fit decay parameters, uncertainties were estimated by varying each parameter in our model until the average RMS deviation between the measured and calculated fluorescence profiles deviated by 5% from that of the best-fit parameters.

In quantifying possible changes with exposure, the two best-fit lifetimes for each sample were combined into a single average lifetime defined by (Zeng et al., 2008):

$$\tau_{avg} = \frac{\alpha_1\tau_1^2 + \alpha_2\tau_2^2}{\alpha_1\tau_1 + \alpha_2\tau_2} . \qquad (3)$$

Figure 9 shows the pre- and post-exposure average lifetimes of QDs with various coatings. The average lifetimes and uncertainties were determined using the average and variation of the best-fit lifetimes across all samples. The post-exposure data were averaged over all non-zero exposures because the data indicated that, to within experimental uncertainty, the average lifetimes of the QDs were independent of both the number of coatings and exposure. Note that this differs from prior observations of structurally similar CdTe QDs coated with CdS shells, in which a lengthening of the radiative lifetime was correlated with increasing shell thickness (Zeng et al., 2008).

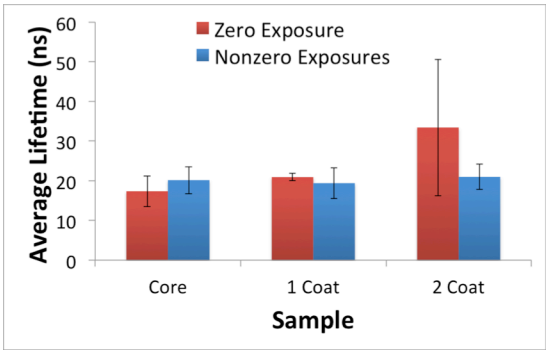

Figure 9. Pre-exposure (red) and post-exposure (blue) average lifetimes for CdTe/ZnS QDs with various numbers of coatings.

CONCLUSION

The optical properties of CdTe quantum dots with varying ZnS shell thicknesses were investigated. We found that as the ZnS shell thickness increased, the absorbance and emission wavelengths were red-shifted. This is indicative of the addition of the ZnS shell and has potential for use as an emission tuning method. We also found that the quantum yield increased as the ZnS shell thickness increased. This increase may be due to the ZnS shell protecting the fluorescent CdTe core from outside factors such as oxygen and light. We found that exposure to incident laser light caused a significant decrease in the fluorescence intensity of the QDs, but not the excitonic peak absorbance or wavelength, peak emission wavelength, or average fluorescence lifetime. The degree of this photobleaching of the fluorescence intensity was reduced for QDs with ZnS coatings indicating that the coatings provided some degree of protection to the CdTe cores. These observations are consistent with photobleaching resulting from photooxidation of the QDs. Our experiments did not include an evaluation of CdTe/ZnS core/shell QDs beyond shell thicknesses of two ZnS monolayers. Therefore, we cannot conclude if these trends continue or decline by increasing the thickness of the ZnS shell even further. However, we believe this initial study warrants further investigation into greater shell thicknesses in an effort to optimize the optical properties of these QDs.

EXPERIMENTAL

Synthesis of CdTe/ZnS QDs

The CdTe/ZnS QDs were synthesized using a modified method published by Zhang et al. (2009). An amount of 51.2 mg of CdO, 280.0 mg of Thiodipropionic Acid (TDPA),

DOI: http://dx.doi.org/10.7710/2168-0620.1057

8.0 mL of 1-octadecene (ODE), and a small stir bar were added to a four-neck round bottom flask attached to a condenser in a nitrogen environment. It was heated to 310 °C and then reduced to 290 °C. In a two-neck round bottom flask attached to a condenser, 5.0 mL of tri-n-octylphosphine (TOP), 127.6 mg of Te powder, and 5.0 mL of ODE were added and heated to 210 °C. Then 4.0 mL of the Te precursor was transferred to the four-neck round bottom flask and allowed to react for two minutes at 290 °C. The core sample was then cooled to about 60 °C and purified using 20 mL of a 1:1 hexanes/methanol mixture in a separatory funnel. Ethanol precipitation and acetone precipitation was used for further purification. Then 10 mL of chloroform was added to the centrifuged pellet in order for UV-Vis spectra collection, and then evaporated using rotary evaporation. Next 70 mg TDPA, 0.5 mL TOP, and 3.5 mL ODE were added to the round bottom flask and the temperature was raised to 135 °C. A ZnS shell precursor was made using 361.9 mg of zinc diethyldithiocarbamate (ZDC), 5.0 mL of TOP, and 5.0 mL of ODE. Then 2.0 mL of the ZnS precursor was added to the reaction mixture and the reaction was continued for 30 minutes, then the temperature was raised to 200 °C for an additional 30 minutes. This cycle continued for three ZnS shell samples. A 2 mL sample was withdrawn for further testing at the end of each cycle. Each sample was purified using the hexanes/methanol mixture and ethanol and acetone precipitation. The final purified samples were diluted with 5 mL of chloroform.

UV-Visible Spectroscopy and Fluorimetry

A Shimadzu UV-1601 spectrophotometer and a Horiba Jobin Yvon Fluoromax-4 were used for optical analysis. Each QD sample was diluted in 3 mL of chloroform in a 1-cm quartz cuvet to an absorbance of 0.1 in order to keep the QD concentration constant. The QD samples were then measured on the fluorimeter using an excitation wavelength of 450 nm and a slit width of 2.5 nm. The samples were tested two days after synthesis.

Quantum Yield

The quantum yield (QY) is defined as the number of visible photons emitted for every UV photon absorbed. The absolute QY can be determined using standard techniques (Williams, Winfield, & Miller, 1983). UV-Vis and fluorescence spectra were collected for the pure solvent (chloroform) and for increasing QD concentrations such that the absorbance at the 450 nm excitation wavelength was in the range of 0 to 0.10. A solution of rhodamine 6G in ethanol was used as a standard. The QY of the QDs was calculated using:

$$\Phi_X = \Phi_{ST}\left(\frac{Grad_X}{Grad_{ST}}\right)\left(\frac{\eta_X^2}{\eta_{ST}^2}\right) \qquad (3)$$

where Φ_{ST} is the QY of the standard, Grad is the slope of the integrated fluorescence intensity versus absorbance curve, and η is the refractive index of the solvent.

Transmission Electron Microscopy

A FEI Tecnai F-20 HR-TEM was used for determining size distributions and lattice spacing for colloidal mercaptopropionic acid quantum dots (MPA-QDs). Samples were prepared by drop-casting the QDs in deionized water onto a Formvar/Carbon 300 mesh copper holey grid (Ted Pella, Inc). The grids were dried in air for three days. Figure 10 shows how TEM images can be used to determine the *d*-spacing by either direct measurement of the distance between each plane or via fast Fourier transform (FFT).

In the FFT case, the d-spacing is calculated by measuring the distance between diffraction points that lie across the circle

DOI: http://dx.doi.org/10.7710/2168-0620.1057

from one another, dividing this distance in half, and then taking the inverse of this answer.

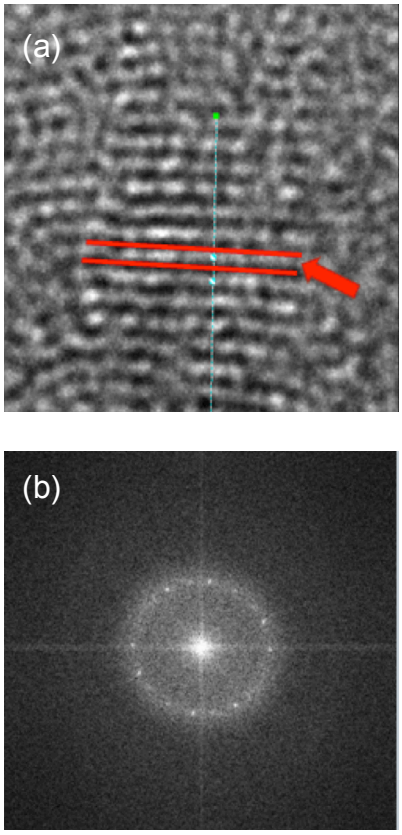

Figure 10. Determining the *d*-spacing by (a) direct measurement on TEM images and (b) FFT measurements.

Photostability Measurements

One milliliter of QDs were diluted in two milliliters of chloroform and then inserted into a 10 mm quartz fluorimeter cell. Absorption and fluorescence emission spectra were recorded before and after various exposure periods. The lasing pulses were provided by a Continuum Panther optical parametric oscillator (OPO) pumped by a seeded, frequency-tripled Continuum Surelite EX Nd:YAG laser. The system produced ~4 ns pulses (10 Hz repetition rate) that were continuously tunable from 410 – 2000 nm and had an approximately gaussian temporal profile. Experiments were performed using a laser wavelength of 435 nm where the QDs exhibited significant absorption. A Coherent Fieldmate power meter and PM30V1Q thermopile sensor were used to measure the energy of the pulses incident on the QD samples. A UniBlitz T132 shutter was used to control the QD exposure to specific numbers of pulses.

The average energy of the incident beam was measured to be 55 mW. QD exposure times ranged from 0 to 320 sec, yielding average exposure energies from 0 to 17.6 J. Between illumination periods, the samples were wrapped in aluminum foil to reduce excess exposure to environmental light. It should be noted that the beam size was such that approximately ¼ of the sample was illuminated during each exposure. The sample was thoroughly mixed after each exposure so that the overexposed QDs were distributed in solution. The temporal profiles of the incident pulses were measured using an Electro-Optics Technology ET-2030 photodiode with a rise time of less than 300 ps. The temporal profile of the portion of the QD fluorescence pulses that were emitted perpendicular to the incident beam direction were measured using a second, identical photodiode. A lens (7.5 cm diameter, 4.5 cm focal length) was used to focus a portion of the fluorescence emission onto the photodiode through a Schott OG-515 long-pass filter that isolated the fluorescence emission wavelength from scattered light from the incident beam. The photodiode signals were analyzed using a 5 Gs/s Tektronix DPO 4104 oscilloscope.

Fluorescence lifetime analysis was performed using a computer program based on the Method of Moments (Isenberg, Dyson, & Hanson, 1973). This numerical technique was selected due to its minimal complexity and computational speed, in addition to the ability of the method to analyze a multi-exponential decay.

DOI: http://dx.doi.org/10.7710/2168-0620.1057

REFERENCES

Dabbousi, B.O., Rodriguez-Viejo, J., Mikulec, F.V., Heine, J.R., Mattoussi, H., Ober, R., Jensen, K.F., & Bawendi, M.G. (1997). (CdSe)ZnS Core-shell quantum dots: Synthesis and characterization of a size series of highly luminescent nanocrystallites. *J. Phys. Chem. B, 101*, 9463-9475. DOI: http://dx.doi.org/10.1021/jp971091y.

Demas, J.N. *Excited State Lifetime Measurements*. Academic Press, New York, 1983.

Eustis, S. & El-Sayed, M.A. (2006). Why gold nanoparticles are more precious than pretty gold: Noble metal surface plasmon resonance and its enhancement of the radiative and nonradiative properties of nanocrystals of different shapes. *Chem. Soc. Rev., 35,* 209-217. DOI: http://dx.doi.org/10.1039/b514191e.

Hines, M.A. & Guyot-Sionnest, P. (1996). Synthesis and characterization of strongly luminescing ZnS-capped CdSe nanocrystals. *J. Physical Chem.*, *100*, 468-471. DOI: http://dx.doi.org/10.1021/jp9530562.

Isenberg, I., Dyson, R., & Hanson, R. (1973). Studies on the analysis of fluorescence decay data by the method of moments. *Biophys. J., 13*, 1090–1115. DOI: http://dx.doi.org/10.1016/S0006-3495(73)86047-3.

Ivanov, S.A., Piryatinski, A., Nanda, J., Tretiak, S., Zavadil, K.R., Wallace, W.O., Werder, D. & Klimov, V.I., (2007) Type-II core/shell CdS/ZnSe nanocrystals: Synthesis, electronic structures, and spectroscopic properties. *J. Am. Chem. Soc.*, *129*, 11708-11719. DOI: http://dx.doi.org/10.1021/ja068351.

Jing, L., Kershaw, S.V., Kipp, T., Kalytchuk, S., Ding, K., Zeng, J., Jiao, M., Sun, X., Mews, A., Rogach, A.L. & Gao, M. (2015). Insight into strain effects on band alignment shifts, carrier localization, and recombination kinetics in CdTe/CdS core/shell quantum dots. *J. Am. Chem. Soc.*, *137*, 2073-2084. DOI: http://dx.doi.org/10.1021/ja5127352.

Kramer, J.I. & Sargent, E.H. (2014). The architecture of colloidal quantum dot solar cells: Materials to devices. *Chem. Rev., 114*, 863−882. DOI: http://dx.doi.org/10.1021/cr400299t.

Nazzal, A.Y., Wang, X., Qu, H., Yu, W., Wang, Y., Peng, X., & Xiao, M. (2004). Environmental effects on photoluminescence of highly luminescent CdSe and CdSe/ZnS core/shell nanaocrystals in polymer thin films. *J. Phys. Chem. B, 108*, 5507-5515. DOI: http://dx.doi.org/10.1021/jp035361q.

Smith, A.M., Mohs, A.M., & Nie, S. (2009). Tuning the optical and electronic properties of colloidal nanocrystals by lattice strain. *Nat. Nanotechnol. 4*, 56-63. DOI: http://dx.doi.org/10.1038/nnano.2008.360.

Talapin, D.V., Mekis, I., Götzinger, S., Kornowski, A., Benson, O., & Weller, H. (2004). CdSe/CdS/ZnS and CdSe/ZnSe/ZnS core-shell-shell nanocrystals. *J. Phys. Chem.*, *108*, 18826-18831. DOI: http://dx.doi.org/10.1021/jp046481g.

van Sark, W.G.J.H.M., Frederix, P.L.T.M., Van den Heuvel, D.J., Gerritsen, H.C., Bol, A.A., van Lingen, J.N.J., de Mello Donega, C., Meijerink, A. (2001). Photooxidation and photobleaching of single CdSe/ZnS quantum dots probed by room-temperature time-resolved spectroscopy. *J. Phys. Chem. B*, *105*,

DOI: http://dx.doi.org/10.7710/2168-0620.1057

8281–8284. DOI: http://dx.doi.org/10.1021/jp012018h.

Waitz, T., Rentenberger, C., & Karnthaler, H.P (2009). Bulk nanostructured intermetallic alloys studied by transmission electron microscopy. In M.J. Zehetbauer & Y.T. Zhu (Eds.), *Bulk Nanostructured Materials* (p. 343). Wiley-VCH: Weinheim. DOI: http://dx.doi.org/10.1002/9783527626892.ch16.

Xu, S.C., Yang, Y.Q., Liu, Y.S., Miao, H., Dong, M., Yang, J., Zhang, J.M., Dai, Z., Zheng, G., Sun, B., Sun, S.Q., & Jiang, Z.Z. (2011). An enhanced luminescent CdTe/ZnS core-shell quantum dot: synthesis, characterization, and its optical properties. In M. Zhou (ed.) Advanced Materials Research Volume 217-218, High Performance Structures and Engineering, Pts 1 and 2, pp. 212-25 Switzerland, TransTech Publications.

Yao, J., Yang, M., & Duan, Y. (2014). Chemistry, biology, and medicine of fluorescent nanomaterials and related systems: new insights into biosensing, bioimaging, genomics, diagnostics, and therapy. *Chem Rev., 114*, 6130−6178. DOI: http://dx.doi.org/10.1021/cr200359p.

Yu, W.W., Qu, L., Wenzhuo, G., & Peng, X. (2003). Experimental determination of the extinction coefficient of CdTe, CdSe, and CdS nanocrystals. *Chem. Mater., 15,* 2854-2860. DOI: http://dx.doi.org/10.1021/cm034081k.

Zeng, Q., Kong, X., Sun, Y., Zhang, Y., Tu, L., Zhao, J. & Zhang, H. (2008). Synthesis and optical properties of Type II CdTe/CdS core/shell quantum dots in aqueous solution via successive ion layer adsorption and reaction. *J. Phys. Chem., 112*, 8587-8593.

Zhang, W., Chen, G., Wang, J., Ye, B., & Zhong, X. (2009). Design and synthesis of highly luminescent near-infrared-emitting water-soluble CdTe/CdSe/ZnS core/shell/shell quantum dots. *Inorg. Chem., 48*, 9723-9731. DOI: http://dx.doi.org/10.1021/ic9010949.

Williams, A. T. R., Winfield, S. A., & Miller, J. N. (1983). Relative fluorescence quantum yields using a computer controlled luminescence spectrometer. *Analyst*, *108*, 1067.